Influence of the fibreglass reinforcement stiffness on the mechanical response of deep tunnel fronts in cohesive soils under undrained conditions

C. di Prisco & L. Flessati
Politecnico di Milano, Milano, Italy

G. Cassani
Rocksoil S.p.A., Milano, Italy

R. Perlo
Officine Maccaferri S.p.A., Zola Predosa, Italy

ABSTRACT: The fronts of tunnels excavated under particularly difficult ground conditions are commonly reinforced by inserting fibreglass pipes. This technique is particularly popular since it is very simple to adapt the reinforcement number/length according to the nature of soils encountered. In this paper, the authors illustrate the results of a 3D FEM numerical campaign aimed at analysing the influence of the reinforcements on the system response, conveniently summarized by employing a suitably normalized front characteristic curve. The numerical analyses were performed by assuming the material to be isotropic, homogeneous and characterized by an elastic-perfectly plastic constitutive relationship. Only undrained conditions are taken into account: the failure locus is defined according to the Tresca criterion and the flow rule is assumed to be associated. The numerical results show that the effectiveness of the inclusions is not related to the absolute value of the inclusion stiffness but to the value of a suitably defined non-dimensional variable. By employing this non-dimensional variable the authors show that it is possible to tailor the reinforcement stiffness according to the nature of the soil encountered.

1 INTRODUCTION

When tunnels are excavated under particularly difficult ground conditions, the front is commonly supported by inserting fibreglass reinforcements in the advance core. This technique had progressively gained popularity in tunnel engineering, since it is very simple to adapt the spatial reinforcements distribution (number, length and pattern), according to the nature of soil encountered.

In the past, numerous authors analysed the mechanical response of reinforced fronts, by employing experimental, numerical and theoretical approaches.

The mechanical response of reinforced tunnel fronts was experimentally investigated by means of small-scale models, by both performing centrifuge (Calvello and Talor (1999), Kamata and Mashimo (2003), Juneja et al. (2010)) and 1g model tests (Yoo and Shin (2003), Shin et al. (2008) and di Prisco et al. (2018a)).

From a numerical point of view, this problem was analysed by performing both FEM (Peila (1994), Yoo & Shin (2003), di Prisco et al. (2018c)) and DEM (Chen et al. (2013)) analyses.

An interesting theoretical approach was proposed in Wong et al. (2000 and 2004), where the front response is assimilated to the one of a spherical cavity excavated in an infinite soil domain subject to a uniform and isotropic state of stress. The presence of the reinforcements

is took into account by defining a suitable homogenized material. Even if this approach allows the estimation of the front displacements, it is not very popular in the tunnel design.

In contrast, in practice, it is common to estimate an "equivalent cohesion" (Grasso et al. (1989)) and to employ the theoretical solutions obtained for unreinforced fronts by employing either the limit equilibrium method (e.g. Horn (1961)) or the limit analysis theory (e.g. Davis et al. (1980), Mühlhaus (1985), Leca & Dormieaux (1990), Augarde et al. (2003)).

An alternative theoretical approach based on the limit equilibrium method is proposed, for granular materials, in Anagnostou & Perazzelli (2015) and, for cohesive materials, in Perazzelli & Anagnostou (2017).

All the theoretical approaches based either on the limit equilibrium method or on the limit analysis theory, are however not suitable for reproducing the mechanical response of deep tunnel fronts in cohesive soils (di Prisco et al. (2018b)). Moreover, these approaches cannot take into consideration the experimentally observed (di Prisco et al. (2018a)) influence of the reinforcement stiffness on the mechanical response of the front.

In this paper, the authors intend to numerically investigate the influence of the reinforcement stiffness on the front response. To this aim, the authors considered a deep tunnel excavated in a homogeneous cohesive soil stratum behaving under undrained conditions and they performed a series of elastic-plastic numerical analyses. The failure condition is defined according to the Tresca criterion and, to avoid volumetric deformations, an associated flow rule is employed. The numerical results are discussed by employing the non-dimensional front characteristic curve, relating the mean value of stress applied on the front and the mean value of the front displacements, proposed in di Prisco et al. (2018b).

The paper is structured as it follows: in §2 the numerical model is described, whereas in §3 and in §4 the numerical analyses results are presented. Finally, in §5 a practical discussion of the influence of the reinforcement stiffness is reported.

2 NUMERICAL MODEL

To study the mechanical response of reinforced tunnel fronts, the authors performed a series of 3D FEM numerical analyses by employing the commercial code Midas GTS NX (http://en.midasuser.com/). The geometry of the numerical model is represented in Figure 1. The tunnel cross section is circular and its diameter is hereafter named D. For the sake of simplicity, the tunnel is assumed to be excavated in a homogeneous cohesive soil stratum, characterized by a constant saturated unit weight (γ_{sat}). The excavation operations are modelled as a reduction in the horizontal geostatic pressure initially applied on the front. For the sake of brevity, the results of only one reinforcement distribution (reported in Figure 1b) and one reinforcement number ($n = 100$) are discussed.

The numerical results are obtained by imposing the following simplifying hypotheses:

(i) the soil mechanical behaviour is assumed to be isotropic elastic-perfectly plastic. Undrained conditions are taken into account: the yield locus is defined according to the Tresca criterion (the undrained strength is hereafter named S_u). To prevent any volumetric deformation, the Poisson's ratio ν_u is imposed equal to 0.5 and the flow rule is assumed to be associated (the dilatancy angle is imposed equal to zero). Both the elastic undrained Young modulus (E_u) and S_u are assumed to be constant along depth;

(ii) only deep tunnels are taken into consideration: the cover/diameter ratio (H/D ratio) is sufficiently large to prevent the plastic domain to get the ground surface;

(iii) the reinforcements are assumed to be characterized by an equivalent circular cross section: their diameter (d) is the diameter of the boreholes drilled to install the reinforcements. The reinforcements are assumed to be constituted by an elastic equivalent material composed by both the reinforcement itself and the concrete grout. The stiffness of this equivalent material is hereafter named E_r. The reinforcements are connected to the soil by means of an elastic-perfectly plastic interface. The failure of the reinforcements is disregarded;

(iv) all the reinforcements are characterized by the same length. Since the actual excavation phases are not modelled, the reinforcement length L represents the minimum length of the reinforcements (before the installation of a new set of reinforcements);

(v) all the reinforcements are assumed to be parallel to the tunnel axis.

The geometrical dimensions of the numerical model (Figure 1) were varied by the authors to assess the reliability of the numerical results. The corresponding numerical results are here omitted for the sake of brevity.

The domain is subdivided in more than 144000 elements: mainly constituted of 8 node hexahedrons and, when necessary for geometrical reasons, of 6 and 5 node pentahedrons (Figure 1). The meshes employed are unstructured and the size of the elements is not uniform within the spatial domain: the mesh size is finer in the part of domain close to the tunnel lining and within the advance core (for a length equal to 2D). To assess the reliability of the numerical results, the authors took into consideration the influence of the spatial discretization on the results. The corresponding numerical results are here omitted for the sake of brevity.

The reinforcements are modelled by means of elastic embedded beam elements (Sadek & Shahrour, 2004). As was previously mentioned, to take into account the soil-reinforcement interface failure, the nodes of the beam elements are connected to the nodes of the soil elements by means of interface elements characterized by an elastic-perfectly plastic behaviour. To reproduce a "quasi rigid"-perfectly plastic interface. The elastic stiffness of the interface elements is significantly larger with respect to the soil stiffness. The maximum bonding stress along the tangential direction between the soil and the beam is assumed to be equal to S_u.

Nil are imposed vertical displacements on the lower boundary, as well as both normal and shear stresses on the upper boundary and stresses on the interior face of the tunnel lining. On the lateral boundaries, horizontal displacements are not allowed, whereas vertical displacements are permitted. The tunnel lining is schematized by means of a rigid plate perfectly constrained to the nodes of the soil domain.
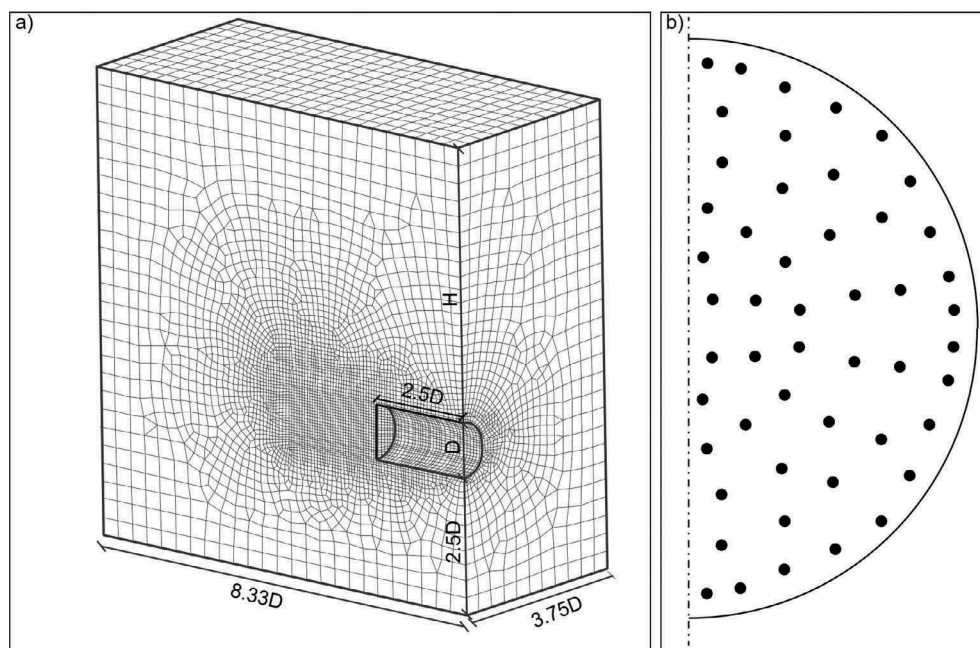

Figure 1.   a) Numerical model and b) adopted reinforcement distribution.

The numerical analyses were performed according to the three following phases:

(i) the initial state of stress is obtained by numerically simulating the stratum formation by keeping constant the geometry and by progressively increasing the gravity. The displacements of the tunnel lining owing to the initial stress conditions are not nil but they are nullified at the beginning of the numerical tests. During this phase, the elements modelling the reinforcements are not introduced in the numerical model;

(ii) the elements corresponding to the reinforcements and to the soil-reinforcement interfaces are activated;

(iii) the initial geostatic linear horizontal stress distribution is progressively nullified.

3 NUMERICAL RESULTS

The numerical results are discussed in the non-dimensional Q_f-q_f plane, introduced in di Prisco et al. (2018b). The non-dimensional stress Q_f and the non-dimensional strain q_f are respectively defined as:

$$Q_f = \left(1 - \frac{\sigma_f}{\sigma_{f0}}\right)\frac{\sigma_{f0}}{S_u} \qquad (1)$$

$$q_f = \frac{u_f}{u_{fr,el}}\frac{\sigma_{f0}}{S_u}, \qquad (2)$$

where σ_f is the mean value of the stress applied on the front, σ_{f0} is the initial (geostatic) value of σ_f, u_f is the average front displacement and $u_{fr,el}$ is the elastic displacements for $\sigma_f = 0$ in the unreinforced case. According to di Prisco et al. (2018b) the employment of these non-dimensional variables is particularly convenient since, in the Q_f-q_f plane the front characteristic curve does not depend on the geometry, on the soil mechanical properties and on the initial state of stress.

The authors performed numerous numerical analyses by considering different reinforcements stiffness values, but, for the sake of clarity, in this section only one reference case (D = 12m, H = 69m, γ_{sat} = 20kN/m^3, S_u = 120kPa, E_u = 50MPa, n = 100, E_r/E_u = 600000, d = 0.15, L = 18m) is initially discussed. The results of the parametric study are reported in §4.
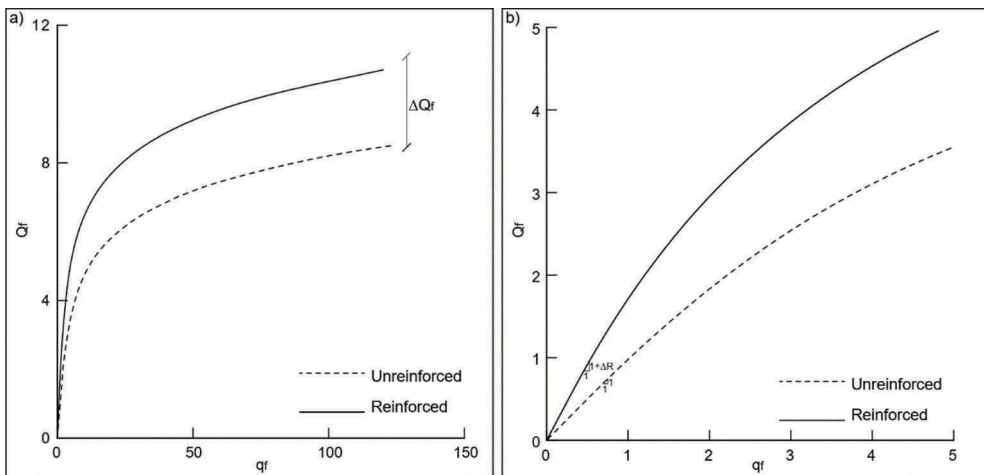

Figure 2. a) comparison between the reinforced and the unreinforced characteristic curve (D = 12m, H = 69m, γ_{sat} = 20kN/m^3, S_u = 120kPa, E_u = 30MPa, n = 100, E_r/E_u = 600000, d = 0.15, L = 18m) and b) detail of Figure 2a for Q_f < 5 and q_f < 5.

In Figure 2a the front characteristic curve obtained for the reference case (solid line) is compared to the corresponding one obtained without reinforcement (dashed line). To better appreciate the initial response, a magnification of Figure 2a is reported in Figure 2b.

The numerical results clearly highlight that the reinforcements severely influence the front characteristic curve. In particular:

- the initial slope of the reinforced curve is significantly larger than the unreinforced one. The initial slope of the unreinforced characteristic curve is 1 (Equations 1 and 2), whereas the initial slope of the reinforced characteristic curve is $1+\Delta R$, where ΔR is the increment in the initial slope with respect to the unreinforced case;
- the amplitude of the initial linear branch of the reinforced curve is larger;
- the final branch of the reinforced curve is almost parallel to the final branch of the unreinforced curve. The vertical distance between the two curves is hereafter named ΔQ_f.

4 PARAMETRIC STUDY

In this section, the influence of the reinforcements stiffness on the front response is numerically investigated. A complete discussion on the influence of the reinforcements (length, number and diameter) on the front mechanical response is reported in di Prisco et al. (2018c). For the sake of generality, a non-dimensional reinforcement relative stiffness is introduced:

$$\bar{E} = \frac{E_r d^2}{E_u L^2}.$$

(3)

This non-dimensional relative stiffness is chosen by assimilating the reinforcements mechanical response to the one of axially loaded piles embedded in an infinite elastic soil domain (Fleming et al. 1985). The characteristic curve in the Q_f-q_f plane is unique for any value of $\bar{E}$. For this reason in Figure 3 each characteristic curve corresponds to a different $\bar{E}$ value. The front characteristic curves obtained for different $\bar{E}$ values are reported in Figure 3a. To better appreciate the initial part of the characteristic curves, a magnification of Figure 3a is reported in Figure 3b.
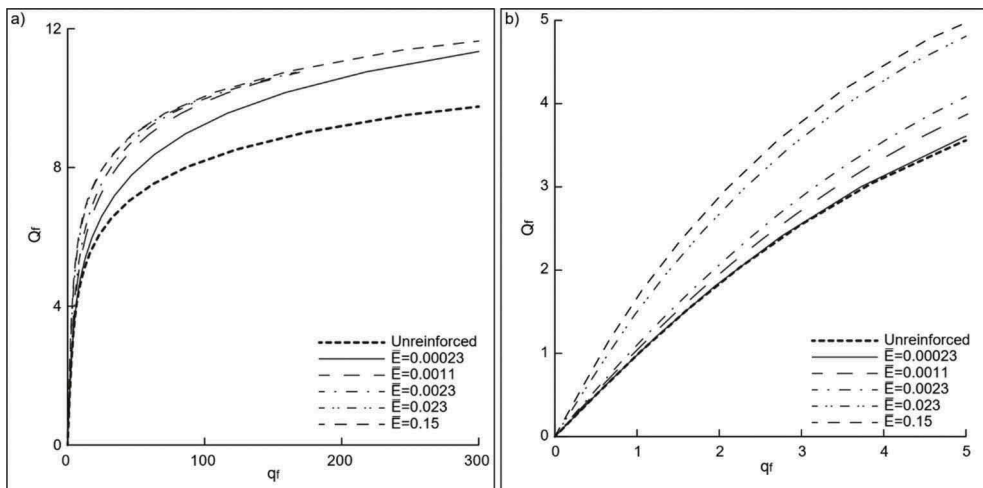

Figure 3. a) influence of the reinforcement stiffness on the front characteristic curve ($D = 12$m, $H = 69$m, $\gamma_{sat} = 20$kN/m^3, $S_u = 120$kPa, $E_u = 30$MPa, $n = 100$, $d = 0.15$, $L = 18$m) and b) detail of Figure 3a for $Q_f < 5$ and $q_f < 5$.
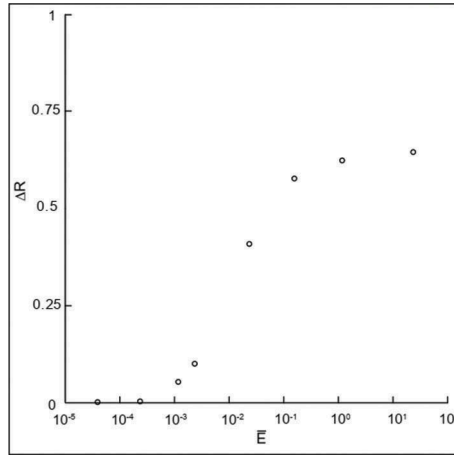
Figure 4. Variation of the initial stiffness of the front characteristic curve with the non-dimensional reinforcement relative stiffness.

The numerical results of Figure 3a and 3b highlight that the reinforcement stiffness significantly influences the initial slope of the characteristic curve: by increasing $\bar{E}$, $\varDelta R$ increases. On the contrary, the final branch of the curves is not influenced by $\bar{E}$ and, therefore, for the sake of simplicity the influence of $\bar{E}$ on $\varDelta Q_f$ is disregarded.

The numerical results of Figure 3 (along with some others omitted in Figure 3 for the sake of clarity), can be summarized by plotting the variation of $\varDelta R$ versus $\bar{E}$ (Figure 4).

As is evident from Figure 4, the results are aligned on a monotonically increasing curve characterized by two horizontal branches.

The horizontal branch for $\bar{E} \rightarrow +\infty$ associated with "rigid" reinforcements testifies that for large $\bar{E}$ values increments in the reinforcement stiffness do not provide significant improvements in the global system response.

The horizontal branch for $\bar{E} \rightarrow 0$ is associated with reinforcements characterized by a stiffness comparable to the soil one and, therefore, the inclusions do not significantly improve the system response.

5 PRACTICAL IMPLICATIONS

In this section the numerical results reported in §4 are employed to discuss, with reference to E_r values typical for practical cases, the influence of the reinforcement stiffness on the front response and in particular on $\varDelta R$. As it was previously mentioned, $\varDelta R$ is influenced by $\bar{E}$ and, therefore, not only by the reinforcement stiffness E_r but also by d, L and E_u. However, for the sake of brevity, d, L and E_u are hereafter kept constant ($d = 0.15$m, $L = 18$m and $E_u = 30$MPa) and only E_r is parametrically varied. The E_u value is chosen to be representative for the case of a tunnel characterized by $D = 12$m and $H = 69$m excavated in a normally-consolidated clay.

The reinforcements commonly adopted in practice are fiberglass pipes grouted in boreholes (Figure 5) and their equivalent stiffness E_r can be calculated by employing the following expression:

$$E_r = \frac{E_g(d^2 - d_{FG,e}^2) + E_{FG}(d_{FG,e}^2 - d_{FG,i}^2) + E_g d_{FG,i}^2}{d^2} \tag{4}$$

where E_g and E_{FG} are the stiffness of the material constituting the grouting and the fibreglass pipes, respectively, whereas $d_{FG,i}$ and $d_{FG,e}$ are the internal and the external fibreglass
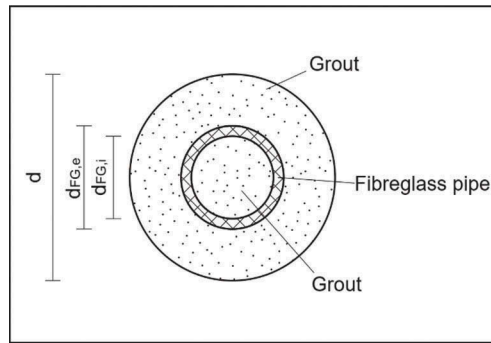
Figure 5. Fibreglass pipe grouted in a borehole.

Table 1. Values for the parametric study.

$d_{FG,i}$ [mm]	$d_{FG,e}$ [mm]	E_{FG} [GPa]	E_g [GPa]
0 ÷ 40	60 ÷ 150	40 ÷ 200	25 ÷ 35

pipe diameter (Figure 5). To study the influence of E_r on the system response, the authors considered different $d_{FG,i}$, $d_{FG,e}$, E_{FG} and E_g values (Table 1).

The influence of $d_{FG,i}$, $d_{FG,e}$, E_{FG} and E_g is discussed in the ΔR-$\bar{E}$ plane in Figures 6a, 6b, 6c and 6d, respectively.

As is evident from Figure 6, in all the cases considered, the $\bar{E}$ values do not belong to the horizontal branches of the numerical curve. This implies that, an increment in the $\bar{E}$ can improve the front response. However, the increase in $\bar{E}$ associated with the variations in $d_{FG,i}$ are practically negligible, whereas by increasing $d_{FG,e}$, E_{FG} and E_g, $\bar{E}$ increases abruptly. Nevertheless, the variation in ΔR, by considering the mechanical and geometrical constraint imposed, is not very marked. This statement is strictly related to stiffness of the soil taken into consideration. Obviously, in case of quite large values of soil/rock stiffness, the variation in ΔR could be quite larger.

Therefore, the numerical results of Figure 6 can also be employed, in a performance based design perspective, to tailor the reinforcements according to the nature of soil encountered. For the sake of simplicity, it can be assumed that the system performance can be summarized with a given ΔR value, which, in its turn, is directly related to one single $\bar{E}$ value. For a given E_u value, E_r can be "designed" (by considering a proper combination of $d_{FG,i}$, $d_{FG,e}$, E_{FG} and E_g) to obtain the target $\bar{E}$ and the corresponding ΔR value.

6 CONCLUSIONS

In this paper, by performing a series of 3D FEM numerical analyses, the authors analysed the influence of the reinforcement stiffness on the mechanical response of deep tunnel fronts in cohesive soil strata under undrained conditions. For the sake of simplicity, the excavation process is modelled as a reduction in the pressure applied on the front. The soil behaviour is modelled by employing an elastic-perfectly plastic constitutive relationship.

The numerical results are analysed by employing a convenient non-dimensional front characteristic curve, relating macroscopic stress and strain variables.
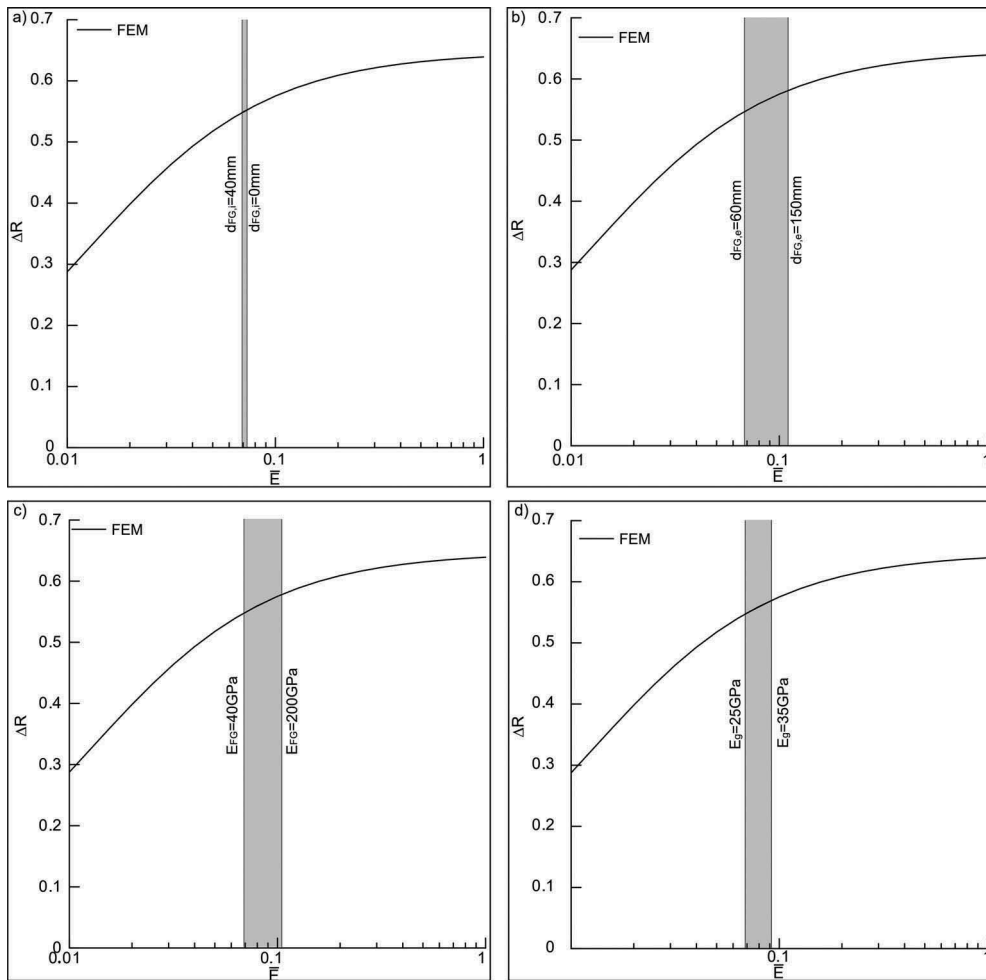
Figure 6. a) influence of $d_{FG,i}$ ($d_{FG,e}$ = 60mm, E_{FG} = 40GPa and E_g = 25GPa), b) influence of $d_{FG,e}$ ($d_{FG,i}$ = 40mm, E_{FG} = 40GPa and E_g = 25GPa), c) influence of E_{FG} ($d_{FG,i}$ = 40mm, $d_{FG,e}$ = 60mm and E_g = 25GPa) and d) influence of E_g ($d_{FG,i}$ = 40mm, $d_{FG,e}$ = 60mm and E_{FG} = 40GPa) for L = 18m, d = 0.15m and E_u = 30MPa.

The numerical results put in evidence that the reinforcement stiffness may significantly influence the front response and, in particular, the initial slope of the front characteristic curves.

Finally, the author show that, in a performance based design perspective, the reinforcements can be tailored on the soil properties and tunnel geometry.

REFERENCES

Anagnostou, G., & Perazzelli, P. (2015). Analysis method and design charts for bolt reinforcement of the tunnel face in cohesive-frictional soils. *Tunnelling and Underground Space Technology* 47:162–181.

Augarde, C. E., Lyamin, A. V., & Sloan, S. W. 2003. Stability of an undrained plane strain heading revisited. *Computers and Geotechnics* 30(5): 419–430.

Calvello, M., & Taylor, R. N. 1999. Centrifuge modelling of a pile-reinforced tunnel heading. *Proc. of Geotechnical Aspect of Underground Construction in Soft Ground*. Rotterdam: Balkema

Chen, R. P., Li, J., Kong, L. G., & Tang, L. J. 2013. Experimental study on face instability of shield tunnel in sand. *Tunnelling and Underground Space Technology*. 33: 12–21.

Davis, E. H., Gunn, M. J., Mair, R. J., & Seneviratine, H. N. 1980. The stability of shallow tunnels and underground openings in cohesive material. *Géotechnique* 30(4): 397–416.

di Prisco, C., Flessati, L. Frigerio, G., Castellanza, R., Caruso, M., Galli, A., Lunardi, P. 2018a Experimental investigation of the time-dependent response of unreinforced and reinforced tunnel faces in cohesive soils. *Acta Geotechnica* 13(3): 651–670.

di Prisco C, Flessati L, Frigerio G, Lunardi P. 2018b A numerical exercise for the definition under undrained conditions of the deep tunnel front characteristic curve. *Acta Geotechnica*, 13 (3): 635–649.

di Prisco, C., Flessati, L. & Porta, D. 2018c Deep tunnel fronts in cohesive soils under undrained conditions: a displacement-based approach for the design of fibreglass reinforcements. *Acta geotechnica*, under review.

Fleming, W. G. K., Weltman, A.J., Randolph, M.F., Elson, W.K. 1985. *Piling engineering*. Surrey University Press, Glasgow and John Wiley, New York.

Grasso, P., Mahtab, A., & Pelizza, S. (1989). Reinforcing a rock zone for stabilizing a tunnel in complex formations. *Proc. Int. congr. Progress innovation in tunnelling*, Toronto, 2, 671–678.

Horn, N. 1961. Horizontaler erddruck auf senkrechte abschlussflächen von tunnelröhren. *Landeskonferenz der ungarischen tiefbauindustrie*, 7–16.

Juneja, A., Hegde, A., Lee, F. H., & Yeo, C. H. 2010. Centrifuge modelling of tunnel face reinforcement using forepoling. *Tunnelling and Underground Space Technology*, 25(4),377–381.

Kamata, H., & Mashimo, H. 2003. Centrifuge model test of tunnel face reinforcement by bolting. *Tunnelling and Underground Space Technology* 18(2–3): 205–212.

Leca, E., & Dormieux, L. 1990. Upper and lower bound solutions for the face stability of shallow circular tunnels in frictional material. *Géotechnique* 40(4): 581–606.

Mühlhaus, H. B. (1985). Lower bound solutions for circular tunnels in two and three dimensions. *Rock Mechanics and Rock Engineering* 18(1): 37–52.

Peila, D. 1994. A theoretical study of reinforcement influence on the stability of a tunnel face. *Geotechnical & Geological Engineering* 12(3): 145–168.

Perazzelli, P., & Anagnostou, G. (2017). Analysis Method and Design Charts for Bolt Reinforcement of the Tunnel Face in Purely Cohesive Soils. *Journal of Geotechnical and Geoenvironmental Engineering* 143(9): 04017046.

Shin, J. H., Choi, Y. K., Kwon, O. Y., & Lee, S. D. (2008). Model testing for pipe-reinforced tunnel heading in a granular soil. *Tunnelling and Underground Space Technology*, 23(3): 241–250.

Wong, H., Subrin, D., & Dias, D. (2000). Extrusion movements of a tunnel head reinforced by finite length bolts—a closed-form solution using homogenization approach. *International journal for numerical and analytical methods in geomechanics*, 24(6),533–565.

Wong, H., Trompille, V., & Dias, D. (2004). Extrusion analysis of a bolt-reinforced tunnel face with finite ground-bolt bond strength. Canadian geotechnical journal, 41(2): 326–341.

Yoo, C., & Shin, H. K. (2003). Deformation behaviour of tunnel face reinforced with longitudinal pipes—laboratory and numerical investigation. *Tunnelling and Underground Space Technology*, 18(4): 303–319.